International Journal of Advanced Robotic Systems

OPEN ACCESS ARTICLE

Gait-based Quadruped Robot Planar Hopping Control with Energy Planning

Regular Paper

Hui Chai[1], Xuewen Rong[1]*, Xingpeng Tang[1] and Yibin Li[1]

1 School of Control Science and Engineering, Shandong University, Jinan, Shandong, China
*Corresponding author(s) E-mail: rongxw@sdu.edu.cn

Received 30 May 2015; Accepted 09 December 2015

DOI: 10.5772/62140

Abstract

To improve the mobility of the quadruped robot, a planar hopping control approach is proposed based on trotting gait. With the proposed approach, three joints of the stance legs are active and the fourth leg is passive. A planar kinematic model of the supporting phase is built and the calculated positions and posture of the torso are used as feedback for motion control. The forces and torque acting at the CoM of the robot torso in the plane are fully controllable and decoupled with the control approach based on a virtual model. The planar motions on three axes are controlled independently. For the hopping control, the total energy in a hopping cycle on the vertical direction is planned according to the desired hopping height of the torso's CoM and the virtual vertical stiffness of the torso is generated using the elastic potential energy of the virtual model. We verify the approach and its robustness using simulation experiments and show the results at the end of this paper.

Keywords Quadrupled Robot, Hopping Control, Active Impedance, Energy Planning, Virtual Model Control

1. Introduction

Following billions of years of evolution, almost all terrestrial animals are legged and can go anywhere on land using these legs. Compared to wheeled and tracked mobile platforms, more agile and versatile four-legged platforms have incomparable superiority in terms of locomotion on complex terrain [1]. On the other hand, four-legged platforms have fewer joints than six-legged ones and are therefore more stable than single-legged and biped ones. Hence, a four-legged robot is a better option for meeting the demands of fast locomotion and transportation on rough terrains such as those presented by forests and mountains [2].

In the past few decades, there has been a developing boom in the area of quadruped robots. BigDog, as one of the most advanced quadruped robots in the world, can traverse a range of complex terrains and represents a milestone in the development of quadruped robots [3]. In addition to BigDog, LS3 was introduced by Boston Dynamics (BDI) as a prototype of a legged supporting vehicle [4]. HyQ from the Italian Institute of Technology (IIT) is another famous quadruped robot platform, but still being developed in the lab [5]. Additionally, JINPOONG from the Korea Institute of Industrial Technology (KITECH) [7] and SCalf from Shandong University (SDU) [8] are also worth noting in the field of quadruped robot research. These platforms are all hydraulic and are the same size as BigDog. Many different approaches to balancing and locomotion control have also been developed to enable these platforms to walk and run on rough terrain via dynamic gait.

In order to further improve the mobility of quadruped robots, some control approaches to genuine running gait have been developed and realized. The duty factor in the supporting phase β [9] of such gaits is less than 0.5. There is no doubt that the three-part control method based on the spring loaded inverted pendulum (SLIP) model presented by Raibert has been successful in terms of balancing and the dynamic locomotion control of legged robots [10]. Such a quadruped running robot achieved a world land speed record for legged robots (6 m/s) in the 1980s [3]. Ahmadi and Buehler presented a stable running control approach based on a one-legged model with hip and leg compliance [11]. Sato and Buehler realized planar hopping control on a one-legged robot with only one actuator [12]. Smith and Poulakakis realized a rotary gallop on SCOUT II [13]. MIT's Cheetah, developed in a biomimetic robotics laboratory (BRL), can gallop at a speed up to 22 km/h in the lab with its compliant mechanism [14,15] and optimally scaled hip-force planning (OSHP) [16]. Shkolnik, Levashov, Manchester and Tedrake presented their bounding approach on rough terrain based on a planar model and the rapidly exploring random tree (RRT) [17]. The BDI cheetah is currently the fastest quadruped robot with a 17.6m/s galloping gait and its improved type, WildCat, can gallop and bound outdoors using its onboard power system [18].

However, neither running-based or one-legged models such as SLIP, or any other approach using a planar model can render all degrees of freedom (DoFs) for the torso controllable.

To solve this problem, a decoupled motion control approach is proposed based on a planar model of supporting phase with trotting gait [1] and virtual model control [19,20]. There is one fore stance leg and one rear stance leg at least in the supporting phase of gait.

By planning the total energy with the desired hopping height and the virtual elastic potential energy of the supporting phase on vertical direction, the virtual stiffness of the supporting phase is generated and applied to the torso's centre of mass (CoM) by active impedance control. Using this approach, it will be easier to control a system integrated with high stiffness active joints and passive energy storage units such as the series elastic actuator (SEA) [21].

In the simplified model, one of four joints on the stance legs of the planar robot is passive during the supporting phase. The planar robot loses redundancy and internal force cannot be set. However, with the control approach, only a small amount of torque is needed on a particular active joint in a real robot system. If the main actuator of this joint malfunctions, the robot can keep moving by using a smaller standby actuator.

This paper is organized as follows: section 2 introduces a simplified planar model and provides the kinematics of the model. Section 3 provides a position and proposed control method for the torso's CoM, based on the presented model. Section 4 presents an energy planning-based hopping control approach and section 5 reports the experimental results obtained from simulations. Finally, section 6 presents conclusions and suggestions for further research.

2. Planar Model for Supporting Phase

When a quadruped robot is running steadily with a trotting gait, the planar model of the supporting phase can be simplified as a planar five-bar linkage as shown in Figure 1, as well as two point-feet contact to the ground. If the mass of the torso is significantly greater than the mass of the legs, the CoM of the robot will be approximately the CoM of the torso. The positions and pose of the CoM are described by (x_b, y_b and θ_b) in the coordinate frame O, the origin of which is set at the rear foot contact point to the ground; θ_b is the pitch angle of the robot torso; q_1, q_2, q_3 and q_4 are the joint angles of the supporting legs.

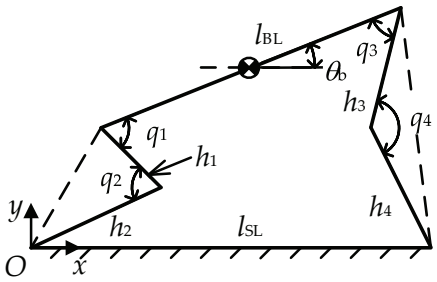

Figure 1. The simplified planar model of the supporting phase, based on trotting gait

The degree of freedom (DoF) of the planar five-linkage is 3 and to enhance the vertical supporting forces and reduce static frictions between the feet and the ground, q_1, q_2 and q_4 are chosen as the active joints. For forward kinematics, the 3-DoF pose of the torso is the function of q_1, q_2 and q_4.

The solution of the kinematic model is divided into two steps as shown in Figure 2.

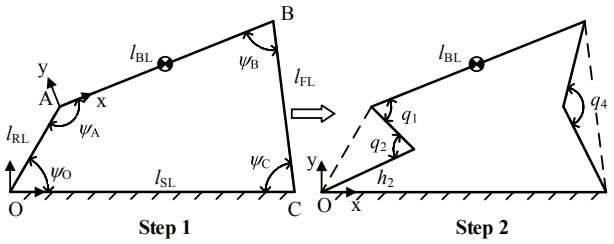

Figure 2. The two steps for modeling flow

Step 1. Solve the kinematics of a planar four-linkage mechanism with l_{RL}, l_{FL} and ψ_A as variables;

Step 2. Substitute the variables in step 2 (q_1, q_2, q_4) for the variables in step 1 (l_{RL}, l_{FL}, ψ_A) and get a solution for the five-bar linkage mechanism.

A basic vector equation can be obtained from step 1 as shown in Figure 2 as follows

$$\overrightarrow{OA} + \overrightarrow{AB} = \overrightarrow{OC} + \overrightarrow{CB}. \tag{1}$$

Let l_{RL}, l_{BL}, l_{SL} and l_{FL} represent the lengths of $\overrightarrow{OA}$, $\overrightarrow{AB}$, $\overrightarrow{OC}$ and $\overrightarrow{CB}$, respectively. ψ_{RL}, ψ_{BL}, ψ_{OC} and ψ_{FL} are the vector angles of the four vectors. In the coordinate frame O and ψ_{BL} is θ_b.

Unlike the three other vector angles, l_{SL} and ψ_{OC} are constant during the supporting phase, because no relative motion is expected between the fore and rear supporting feet in a stable supporting phase. When the robot trots on flat ground, ψ_{OC} can be regarded as zero; all the results presented in this paper are based on $\psi_{OC}=0$, $\psi_{RL}=\psi_O$, $\psi_{BL}=\theta_b$ and $\psi_{FL}=\pi-\psi_C$.

Thus, using the geometric method, the forward solution of position in step 1 can be calculated as:

$$\begin{cases} \theta_b &= \psi_O + \psi_A - \pi \\ x_b &= l_{RL}c_O + \frac{1}{2}l_{BL}c_b \\ y_b &= l_{RL}s_O + \frac{1}{2}l_{BL}s_b \end{cases}, \tag{2}$$

where $s_O=\sin\psi_O$, $c_O=\cos\psi_O$, $s_b=\sin\theta_b$, $c_b=\cos\theta_b$ and ψ_O is the angle shown in Figure 2 and cannot be measured, but can be calculated as:

$$\begin{aligned} \psi_O &= \psi_{O1} + \psi_{O2} \\ \psi_{O1} &= \arccos\left(\frac{l_{RL} - 2l_{BL}c_A}{\sqrt{l_{BL}^2 + l_{RL}^2 - 2l_{BL}l_{RL}c_A}}\right) \\ \psi_{O2} &= \arccos\left(\frac{l_{SL}^2 + l_{BL}^2 + l_{RL}^2 - l_{FL}^2 - 2l_{BL}l_{RL}c_A}{2l_{SL}\sqrt{l_{BL}^2 + l_{RL}^2 - 2l_{BL}l_{RL}c_A}}\right) \end{aligned}, \tag{3}$$

where $c_A=\cos\psi_A$.

In step 2, the variables can be substituted as q_1, q_2 and q_4 by Eq. (4),

$$\begin{cases} l_{RL} = \sqrt{h_1^2 + h_2^2 - 2h_1h_2c_2} \\ l_{FL} = \sqrt{h_3^2 + h_4^2 - 2h_3h_4c_4} \\ \cos\psi_A = \frac{h_1c_1 - h_2c_{2-1}}{l_{RL}} \\ \cos\psi_B = \frac{h_3c_3 - h_4c_{4-3}}{l_{FL}} \end{cases}, \tag{4}$$

where $c_1=\cos q_1$, $c_2=\cos q_2$, $c_3=\cos q_3$, $c_4=\cos q_4$, $c_{2-1}=\cos(q_2-q_1)$, $c_{4-3}=\cos(q_4-q_3)$, h_1, h_2, h_3 and h_4 are the lengths of the links of both front and rear legs.

The forward kinematics of the planar model can be obtained by Eq. (2)-(4).

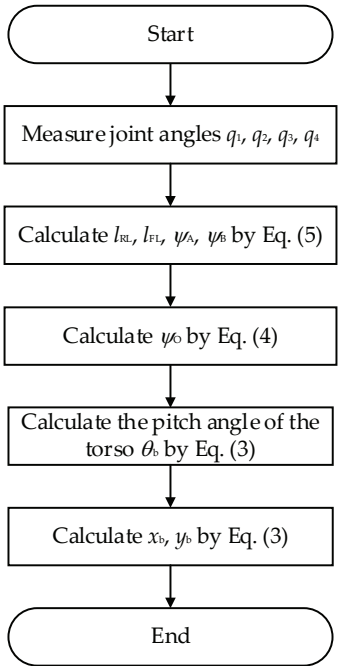

Figure 3. Calculating flow diagram of the kinematic model

The calculating flow of the forward kinematics is shown in Figure 3. l_{SL} is calculated at the very beginning of the supporting phase with the pitch angle sensing of the torso.

The speed form of the model is also solved by the two steps shown below:

$$\begin{cases} \begin{pmatrix} \dot{x}_b \\ \dot{y}_b \\ \dot{\theta}_b \end{pmatrix} &= J_1 \begin{pmatrix} \dot{l}_{FL} \\ \dot{l}_{RL} \\ \dot{\psi}_A \end{pmatrix} \\ \begin{pmatrix} \dot{l}_{FL} \\ \dot{l}_{RL} \\ \dot{\psi}_A \end{pmatrix} &= J_2 \begin{pmatrix} \dot{q}_1 \\ \dot{q}_2 \\ \dot{q}_4 \end{pmatrix} \end{cases}. \tag{5}$$

Compared to deriving the forward kinematic equations, solving the speed form of the vector equation is easier than obtaining the angular velocity of CoM. The speed form of Eq. (1) in coordinate frame A, which is fixed to link AB, can be written as:

$$\begin{aligned} &\dot{l}_{RL}e^{-i\psi_A} - il_{RL}\dot{\psi}_A e^{-i\psi_A} - il_{SL}\dot{\theta}_b e^{-i\theta_b} = \\ &\dot{l}_{FL}e^{-i(\pi-\psi_B)} + il_{FL}\dot{\psi}_B e^{-i(\pi-\psi_B)} \end{aligned}. \tag{6}$$

By solving Eq. (6), the pitch angle speed can be obtained as:

$$\dot{\theta}_b = \frac{1}{l_{SL} s_{bB}} \begin{pmatrix} 1 & c_{AB} & -l_{RL} s_{AB} \end{pmatrix} \begin{pmatrix} \dot{l}_{FL} \\ \dot{l}_{RL} \\ \dot{\psi}_A \end{pmatrix}, \tag{7}$$

under the condition of

$$\begin{cases} s_A & \neq 0 \\ s_{bB} & \neq 0, \\ l_{SL} & \neq 0 \end{cases}$$

where $s_{bB}=\sin(\theta_b+\psi_B)$, $c_{AB}=\cos(\psi_A+\psi_B)$ and $s_{AB}=\sin(\psi_A+\psi_B)$. This result will almost always be met when the robot is walking and running.

The linear speed of the CoM can be obtained by substituting Eq. (7) into the derivative of Eq. (2), as shown in Eq. (8)

$$J_1 = \frac{1}{l_{SL} s_{bB}} \begin{pmatrix} J_{11} \\ J_{12} \\ J_{13} \end{pmatrix}, \tag{8}$$

where,

$$J_{11}{}^T = \begin{pmatrix} -l_{RL} s_O - \frac{1}{2} l_{BL} s_b \\ l_{SL} s_{bB} c_O - l_{RL} c_{AB} s_O - \frac{1}{2} l_{BL} c_{AB} s_b \\ \left(l_{SL} s_{bB} s_O + l_{RL} s_{AB} s_O + \frac{1}{2} l_{BL} s_{AB} s_b \right) l_{RL} \end{pmatrix},$$

$$J_{12}{}^T = \begin{pmatrix} l_{RL} c_O + \frac{1}{2} l_{BL} c_b \\ l_{RL} c_{AB} c_O + l_{SL} s_{bB} s_O + \frac{1}{2} l_{BL} c_{AB} c_b \\ -\left(l_{RL} s_{AB} c_O + l_{SL} s_{bB} c_O + \frac{1}{2} l_{BL} s_{AB} c_b \right) l_{RL} \end{pmatrix},$$

$$J_{13}{}^T = \begin{pmatrix} 1 \\ c_{AB} \\ -l_{RL} s_{AB} \end{pmatrix}.$$

J_2 can be calculated by deriving Eq. (4) as follows:

$$J_2 = \begin{pmatrix} 0 & 0 & \frac{h_3 h_4 s_4}{l_{FL}} \\ 0 & \frac{h_1 h_2 s_2}{l_{RL}} & 0 \\ \frac{h_1 s_1 + h_2 s_{2-1}}{l_{RL} s_A} & \frac{h_1 h_2 s_2 c_A - h_2 l_{RL} s_{2-1}}{l_{RL}^2 s_A} & 0 \end{pmatrix}, \tag{9}$$

where $s_1=\sin q_1$, $s_2=\sin q_2$, $s_4=\sin q_4$, $s_{2-1}=\sin(q_2-q_1)$. The Jacobin in Eq. (10) is $\mathbf{J}=\mathbf{J}_1 \cdot \mathbf{J}_2$ and the speed solution for the planar model is:

$$\begin{pmatrix} \dot{x}_b \\ \dot{y}_b \\ \dot{\theta}_b \end{pmatrix} = J \begin{pmatrix} \dot{q}_1 \\ \dot{q}_2 \\ \dot{q}_4 \end{pmatrix}. \tag{10}$$

3. Motion Control Based on Virtual Model

A gait cycle is determined by motion during the supporting phase. In this section, a motion control approach is introduced to implement the compliant motion of the torso on three axes, based on virtual model control and the solutions noted in section 2.

3.1 The virtual model control based on the planar model

In the planar motion control, x_{db} and y_{db} (the desired torso's CoM positions along the x and y axes of the coordinate frame O) and β_{db} (the desired torso pitch angle along the z -axis of the coordinate frame O) serve as reference inputs. The control forces and torque f_x, f_y, τ_z are calculated by the virtual stiffness-damping model, which is shown in Figure 4.

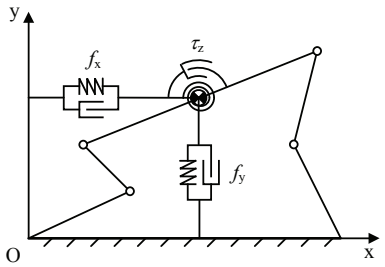

Figure 4. The planar 3-DoF virtual stiffness-damping model

The control law of the virtual model is shown as:

$$\begin{cases} f_x &= k_{sx}\left(x_{db} - \hat{x}_b\right) - k_{dx}\dot{\hat{x}}_b \\ f_y &= k_{sy}\left(y_{db} - \hat{y}_b\right) - k_{dy}\dot{\hat{y}}_b, \\ \tau_z &= k_{sz}\left(\theta_{db} - \hat{\theta}_b\right) - k_{dz}\dot{\hat{\theta}}_b \end{cases} \tag{11}$$

where x_{db}, y_{db} and θ_{db} are the desired positions and present the values of the torso's CoM, $\hat{x}_b$, $\hat{y}_b$, $\hat{\theta}_b$ are the detected positions of the torso's CoM, and $\dot{\hat{x}}_b$, $\dot{\hat{y}}_b$ and $\dot{\hat{\theta}}_b$ are the detected speeds of the torso's CoM. The speed can also be obtained by deriving the detecting position. k_{sx}, k_{dx}, k_{sy}, k_{dy}, k_{sz}, k_{dz} are the virtual stiffness and damping of the torso's position and rotation along the x, y and z axes of the coordinate frame O.

Of course, the control forces f_x, f_y and τ_z are all virtual forces, serving as outputs of the virtual model controller,

not the real actuating torques on the joint. It is necessary to receive the transformation function from the control force space in order to actuate force space for control in practice.

However, the robot feet are not actually fixed on the ground; here we render f_x and τ_z as bounded with f_y, shown as follows:

$$f_x = \begin{cases} \mu_{xy} f_y & k_{sx}\left(x_{db} - \hat{x}_b\right) - k_{dx}\dot{\hat{x}}_b \geq \mu_{xy} f_y \\ -\mu_{xy} f_y & k_{sx}\left(x_{db} - \hat{x}_b\right) - k_{dx}\dot{\hat{x}}_b \leq -\mu_{xy} f_y \end{cases}$$
$$\tau_z = \begin{cases} \mu_{zy} f_y & k_{sz}\left(\theta_{db} - \hat{\theta}_b\right) - k_{dz}\dot{\hat{\theta}}_b \geq \mu_{zy} f_y \\ -\mu_{zy} f_y & k_{sz}\left(\theta_{db} - \hat{\theta}_b\right) - k_{dz}\dot{\hat{\theta}}_b \leq -\mu_{zy} f_y \end{cases}, \quad (12)$$

where the parameters μ_{xy} and μ_{zy} have to be adjusted in the experiments according to terrain type and the ZMP condition. In this paper, f_y is a fundamental variable for maintaining cyclical hopping; a significant f_x and τ_z can be avoided at the beginning and end of the supporting phase by bounding them with f_y.

It is noted that the mass of torso is far greater than the mass of the legs discussed in section 2. Therefore, the following assumption is made:

Assumption: The forces for driving the links of legs can be ignored compared to forces driving the torso in the supporting phase of the gait.

According to the above assumption, the transformation function from control force space to actuating force space should be the Jacobin matrix as shown below:

$$\boldsymbol{T}_{\text{Joint}} = \boldsymbol{J}^{\text{T}} \boldsymbol{u}_b, \quad (13)$$

where $\mathbf{u}_b = (f_x \quad f_y \quad \tau_z)^{\text{T}}$ is the virtual control force acting at the CoM of the torso and $\mathbf{T}_{\text{Joint}} = (\tau_1 \quad \tau_2 \quad \tau_4)^{\text{T}}$ is the joint torques actuating on q_1, q_2 and q_4.

3.2 Position control based on the virtual model

According to the description above, a virtual model based on a force control block diagram is given in Figure 5.

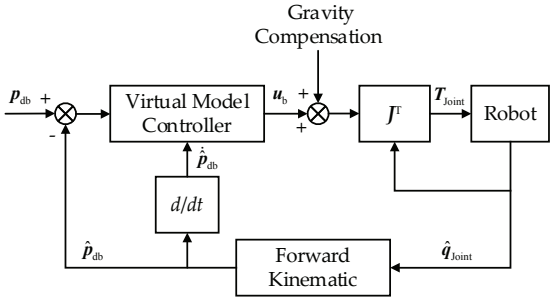

Figure 5. The block diagram for the motion control

p_{db} contains three elements, $(x_{db}, y_{db}$ and $\theta_{db})$ as the desired position of the CoM. CoM position feedback p_b is calculated by the forward kinematics of the planar model via the detected joint angles q_{Joint}. The virtual control force u_b is calculated by the control law of Eq. (11) as the output of the virtual model controller. The gravity compensation in coordinate frame O is a constant represented as $(0 \quad m_b g \quad 0)^{\text{T}}$. The final, real actuating torque T_{Joint} is calculated by Eq. (12) as the input of the robot.

Because the robot feet only just make contact with the ground, the feet may take off. When a foot takes off, the virtual model would get unavailable and cause the locomotion and hopping control to fail. In Figure 6, when ZMP (zero moment point) of the robot is at ZMP1, there is a large margin for adjusting the pitch angle and horizontal acceleration of the robot torso by f_x and τ_z. When ZMP comes close to ZMP2, the stability margin becomes small. It is very easy to make normal active force on the feet get to zero or a positive when applying some required f_x and τ_z, as calculated by Eq. (11), which will cause the foot to move off of the ground. This situation cannot be avoided completely by Eq. (12); after all, it does not bound the active forces of the feet directly. Therefore, ZMP getting too close to ZMP2 when planning the accelerations of the torso's CoM should be avoided. In this paper, no planning regarding the trajectory of the robot's ZMP is presented; however, it is shown that the longitudinal stability margin can be adjusted in order to keep robot hopping steady by changing a parameter of k_{SL}; this will be further addressed in section 4.4.

Slip is another problem that may cause the control approach to fail. However, slip is related to the normal supporting force and friction factors between the feet and the ground. This is a rather complex problem for a legged robot, the details of which are beyond the scope of this paper. In the simulation, the friction coefficient between the feet and the ground does not change and is set to 1.

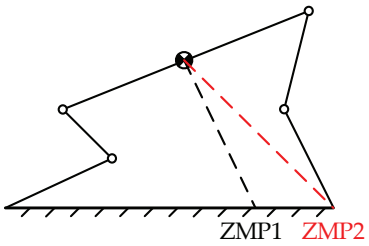

Figure 6. Stability analysis for planar motion

4. Hopping Control with Energy Planning

4.1 Hopping process analysis

For hopping control, a cycle is divided into two phases, referred to as the supporting phase and swing phase,

shown in Figure 7. The definitions for symbols are shown in Table 1. The supporting phase lasts from both feet touching down onto the ground to one of the feet leaving the ground. Swing phase is the time between the end of the previous supporting phase and the next.

Hopping control should only be effected during the supporting phase. The hopping cycle is controlled by variable stiffness along the y -axis of the coordinate frame O based on energy planning of the virtual model. The supporting phase is divided into two periods, i.e., the compressing period and releasing period. The compressing period lasts from the beginning of the supporting phase to the time where the CoM of the robot reaches the lowest position on the y -axis. During this period, the virtual spring on the y -axis stores energy that is also virtual. The energy of hopping motion is charged by changing the vertical virtual stiffness. The releasing period lasts from the end of the compressing period to the end of the supporting phase. During this period, the virtual spring releases the energy and transfers it to kinetic and gravitational potential energy.

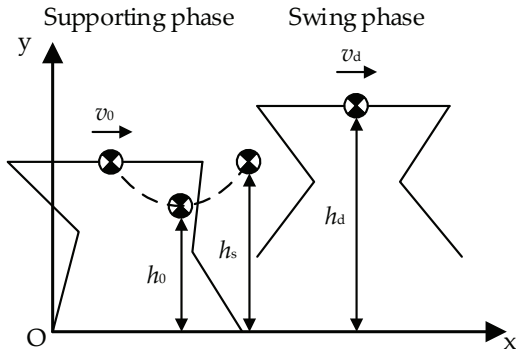

Figure 7. Analysis of the hopping process

Since the controlling virtual forces are decoupled, the kinetic energies and rotational kinetic energy along the x, y and z axes can be controlled separately. This is the primary difference from the SLIP model. The horizontal hopping speed is controlled by f_x, hopping height and hopping cycle time are both controlled by f_y and the pitch of the torso is controlled by τ_z.

Symbol	*Definition*
h_0	The desired minimum CoM height in the supporting phase
h_s	The CoM height at the time of supporting phase transmitting to swing phase equals height at time of swing phase transmitting to supporting phase during stable hopping
h_d	The desired hopping height
v_0	The horizontal velocity at the time of touchdown
v_d	The desired horizontal velocity

Table 1. Symbol definition of the hopping process

4.2 Hopping height and cycle control

During the supporting phase, the control law of f_y is still a virtual spring (Eq. (11)) with no damping (k_{dy}=0). There is no acting non-conservative force; therefore, the total energy E_d, which includes kinetic energy E_{ky}, gravitational potential energy E_{pg} and virtual elastic potential energy E_{pey} is constant as follows:

$$E_d = E_{ky} + E_{pg} + E_{pey}, \tag{14}$$

where,

$$\begin{aligned} E_{ky} &= \frac{1}{2} m_b \dot{y}_b^{\,2} \\ E_{pg} &= -m_b g y_b \\ E_{pey} &= \begin{cases} 0 & y_b \geq h_s \\ -\frac{1}{2} k_{sy} \left(y_b - h_s \right)^2 & y_b < h_s \end{cases} \end{aligned},$$

m_b is the mass of the torso, g is acceleration of gravity and the zero potential level is set at a height of y=0.

During the compression period, the desired total energy consists of the virtual elastic potential energy and the gravitational potential energy at the desired minimum CoM height point as follows:

$$E_d = -\frac{1}{2} k_{sy} \left(h_0 - y_{b0} \right)^2 - m_b g h_0,$$

where, y_{b0} is the height of the torso at the beginning of the compression period.

Thus, the virtual stiffness k_{sy} in the control law can be calculated as:

$$k_{sy} = \frac{\dot{y}_b^{\,2} - 2g\left(y_b - h_0 \right)}{\left(y_b + h_0 - 2y_{b0} \right)\left(y_b - h_0 \right)} m_b. \tag{15}$$

When y_b comes very close to h_0, k_{sy} calculated by Eq. (15) will become very large due to the error of the energy and the small denominator. In such a situation, the equation for calculating k_{sy} is switched to Eq. (16). By doing this, k_{sy} is not connected to y_b, but only related to the energies at the start of the compression period.

$$k_{sy} = \frac{v_{0y}^{\,2} - 2g\left(y_{b0} - h_0 \right)}{\left(h_0 - y_{b0} \right)^2} m_b, \tag{16}$$

where v_{0y} is the vertical speed of the torso at the beginning of the compression period.

During the release period, the desired total energy E_d is set to the gravitational potential energy at the desired hopping height h_d as follows:

$$E_d = -m_b g h_d.$$

The equation for virtual stiffness k_{sy} during the release period is:

$$k_{sy} = \frac{2g\left(h_d - y_b\right) + \dot{y}_b^{\,2}}{\left(y_b - h_s\right)^2} m_b. \tag{17}$$

Similar to stiffness planning in the compression period, when y_b gets close to h_s, the denominator of Eq. (17) is close to zero. Thus, stiffness can be calculated with the desired gravitational potential energy at hopping height as follows:

$$k_{sy} = \frac{2g\left(h_d - h_0\right)}{\left(h_0 - h_s\right)^2} m_b. \tag{18}$$

The entire hopping cycle control block diagram is illustrated in Figure 8.

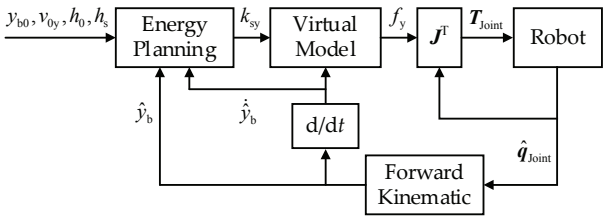

Figure 8. Block diagram of the hopping cycle control

4.3 Horizontal velocity control

The horizontal velocity of the torso is controlled by f_x in the supporting phase and maintained during the swing phase. The control law for f_x during the supporting phase of a hopping cycle is shown as:

$$f_x = k_v\left(v_d - \dot{x}_b\right), \tag{19}$$

where k_v denotes the force/speed gain. Fewer hopping cycles are taken by robot to speed up to the desired velocity at a higher k_v.

In this paper, the desired pitch angle is zero. The control law of τ_z is still calculated using Eq. (11). f_x and τ_z are still bounded by f_y as Eq. (12).

4.4 Swing foot trajectory planning

The swing time of the swing phase t_f in ideal cyclical hopping is only determined by the vertical takeoff velocity of the torso v_{fy} and is based on the assumption that the air resistance and changes to the configuration of the robot during flight can be ignored.

$$t_f = -\frac{2v_{fy}}{g}. \tag{20}$$

With trotting gait, the swing time of a foot equals double t_f plus the time of another supporting phase. In this paper, our research observed planar locomotion; as such, there is only one supporting phase and one swing phase in a gait cycle, and the swing time of each foot is t_f.

However, we cannot certainly know when the foot touches down on the ground, especially on rough terrain. However, the rising time of the swing phase is certain once a foot of robot leaves the ground and this takes half the time of t_f. Therefore, we let the feet swing to the desired position for the next supporting phase during this rising time.

The trajectory of the swinging feet in the coordinate frame fixed at the CoM of the torso is planned using a cubic curve to avoid the mutation of acceleration, as shown in Eq. (21)

$$\begin{cases} T(t) & = a_3 t^3 + a_2 t^2 + a_1 t + a_0 \\ \dfrac{dT(t)}{dt} & = 3a_3 t^2 + 2a_2 t + a_1 \end{cases}, \tag{21}$$

where a_0, a_1, a_2 and a_3 are the parameters of the swing trajectory and they can be calculated using the measured feet positions, velocities at the very beginning of swing, and the final desired feet positions and velocities.

For trajectory planning, we let the step length be adjusted by the horizon velocity of the torso at the time of taking off, which can be shown as follows:

$$T_x\left(\frac{t_f}{2}\right) = k_{SL} v_{fx} \pm \frac{l_{BL}}{2}, \tag{22}$$

where k_{SL} is the scaling factor between the step length and v_{fx}, which is the measured horizon take-off velocity, the positive half torso length for the front foot and the negative length for the rear foot. By adjusting k_{SL}, the CoM of the torso can achieve a suitable workspace of kinematics, as well as the adequate longitudinal stability margin of ZMP in the supporting phase.

A low gain PD control is used as the swing foot position control. Based on the assumption in section 3.1, the gain of the PD control can be very low. Shock will not spread to the torso, even is there is unexpected impact between the foot and the ground.

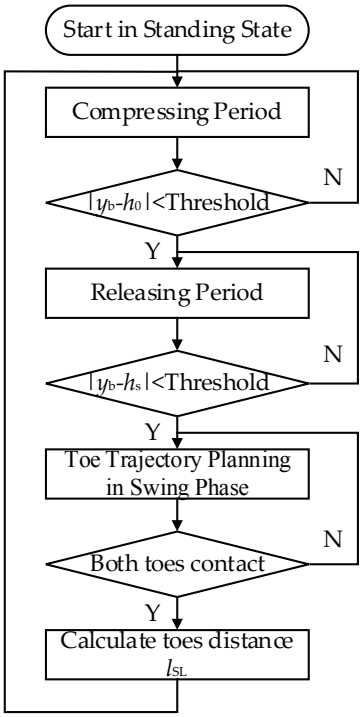

Figure 9. Control flow diagram of a hopping cycle

4.5 Control flow of the hopping cycle

The entire hopping cycle control flow diagram is shown in Figure 9 and is unidirectional. Once moving to the next phase or period, it never falls back to the former phase or period. It is therefore unnecessary to worry about oscillation between two neighboring statuses.

In the control flow, a hopping cycle is divided into a compressing period and a releasing period in the supporting phase and swing phase. Whether the flow is in the supporting phase or in the swing phase is determined by the touch sensing on each foot. Once the flow moves into the supporting phase, l_{SF} is calculated first. Pitch angle sensing is needed to calculate l_{SF}.

During the supporting phase, l_{SF} should be a constant if there had been relatively stationary contact between the feet and the ground. Thus, the unexpected interactions between the feet and the ground, such as slipping, can also be established by calculating l_{SF} during the supporting phase.

5. Simulation and Results

To verify the performance of the proposed motion control and hopping control approach, we built a virtual testing system based on Webots 6.4.1, as shown in Figure 10. The motion of the robot is constrained in a plane by two linear motion guides. The torso length (l_{BL}) is 0.5m and the lengths of the leg links (h_1, h_2, h_3, h_4) are all 0.25 m. To satisfy the assumption in section 3.1, the mass of the torso link is set to 5 kg and the mass of each leg link is set to 0.005 kg, which is significantly less than the mass of the torso. The positions on the x and y axes, and the pitch angle on the z -axis of the robot torso are measured using the frame. Two force sensors located on every foot are used for contact sensing.

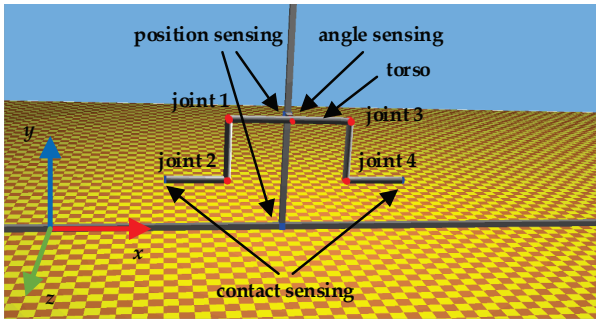

Figure 10. The virtual testing system and simulation environment

The planar motion and hop of the five-linkage system is demonstrated in the simulation. We conducted two groups of simulated experiments to verify the effectiveness of the proposed locomotion control and the hopping control approach.

5.1 Simulated results in motion control

To verify the presented kinematic model, we let the robot stand on the ground in the simulated environment and the CoM of the robot torso track the desired sine curves on the x, y and z axes, with the force control approach as stated in section 3.1. The parameters in Eq. (11) are estimated by the desired position and single rigid body dynamics of the torso first and then adjusted during the tests.

Parameter	*Unit*	*Value*
k_{sx}	N/m	15000
k_{dx}	N/(m/s)	140
k_{sy}	N/m	15000
k_{dy}	N/(m/s)	275
k_{sz}	N·m/rad	15000
k_{dx}	N·m/(rad·s^{-1})	130
μ_{xy}	1	0.1
μ_{zy}	1	0.1

Table 2. The parameters used in motion control

As the simulation result shows, the position along the x and y axes, and the angular position on the z -axis are shown in Figure 11. The blue curves are the desired values and the red curves are measured by the linear motion guides as the real value of the torso pose. The parameters used here are shown in Table 2.

With a group of high impedance parameters, the desired and measured curves are shown to almost overlap. Motion

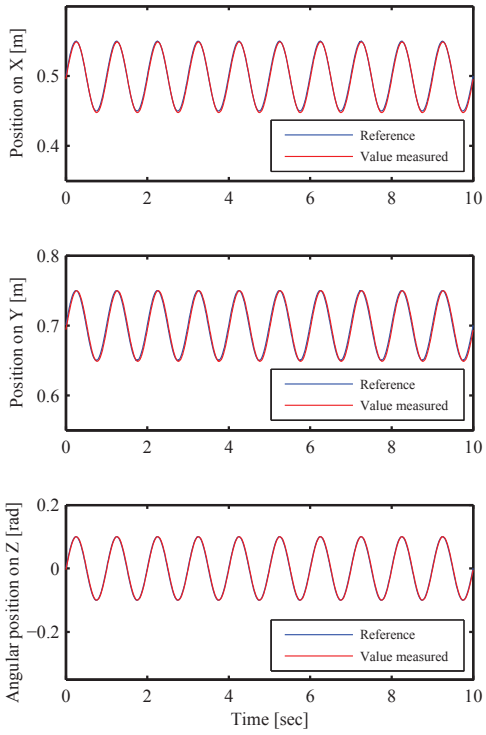

Figure 11. Position and pitch angular curves of the torso's CoM under locomotion control along the x, y and z axes in the coordinate frame O with both feet contacting to the ground

control is also verified by this simulation experiment. However, the motion in the experiment lacks compliance due to the use of such high impedance parameters.

5.2 Simulated results for hopping control

In the hopping experiment, the virtual control forces f_x and f_y are generated via stiffness planning and the speed control method. What needs to be adjusted are k_{sz}, k_{dz} (the parameters of τ_z), μ_{xy}, μ_{zy} (the parameters of the contact bounding function), k_v (the force/speed gain in Eq. (20)) and k_{SL} (the scaling factor between the step length and the measured horizontal take-off velocity in Eq. (22)).

The experiments were conducted with a horizontal robot velocity (v_d) of 2 m/s. Due to the impacts occurring at the beginning of the compressing period, we used a different μ_{zy} in the compressing period and the releasing period to hold the pitch angle of the torso. The parameters are shown in Table 3.

The CoM velocity and position curves of the robot torso on three axes are shown in Figure 12. The red and blue curves are the real values measured by the linear guides and the feedback values calculated by the forward kinematic model. The calculated values are only available during the supporting phase; we stopped refreshing the calculated values and set them to the initial values during the swing phase, so that the blue curves are discontinuous.

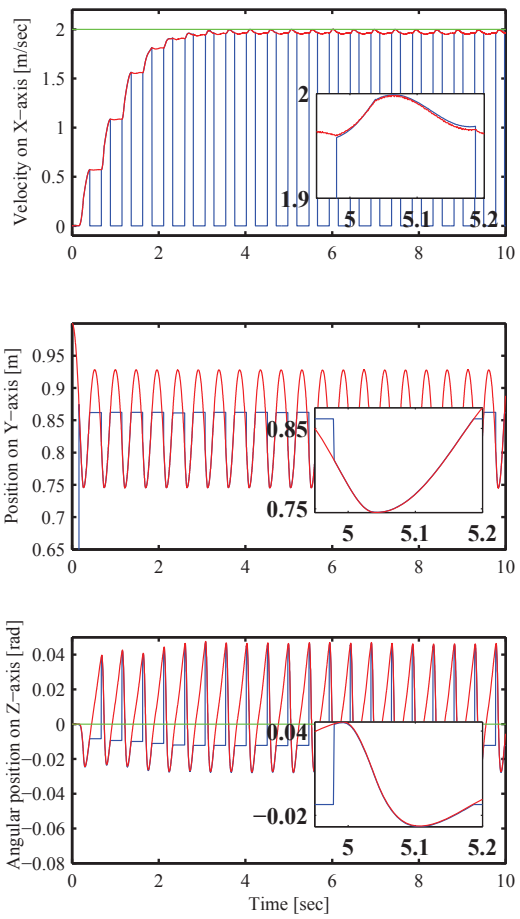

Figure 12. Velocity and position curves of the robot torso's CoM with the hopping control, velocity along the x -axis, position along the y -axis and angular position along the z -axis in the coordinate frame O, as shown in Figure 10. The curves drawn in red are the values measured by the two guides, the blue curves are calculated by the forward kinematics and the green curves are the desired values.

Parameter	*Unit*	*Value*
h_d	m	0.746
h_0	m	0.87
h_s	m	0.93
k_{sz}	N·m/rad	500
k_{dz}	N·m/(rad·s^{-1})	20
μ_{xy}	1	0.1
μ_{zy} (during Compressing Period)	1	0.1
μ_{xy} (during Releasing Period)	1	0.195
k_v	N/(m·s^{-1})	25
k_{SL}	m/(m·s^{-1})	0.08

Table 3. The parameters used in hopping control with a horizontal velocity of 2 m/s

According to the velocity curves on the x -axis, the speed is up to the desired input (2 m/s) at the ninth hopping cycle. Due to the high values of k_{sz} and k_{dz}, the angular position

curves on the z -axis are not smooth, and using the lower values will cause a more intense vibration on the z -axis. Therefore, the values of k_{sz} and k_{dz} need to be adjusted according to the requirement of the torso's pose stability.

The evolution of the vertical stiffness of the virtual model is shown in Figure 13. The speed becomes higher, the energy loss caused by the shock from the feet also becomes higher and more energy is needed to support the buffering period. Thus, stiffness during buffering period is bigger than during the releasing period. When y_b reaches close to h_0 and h_s, the virtual stiffness calculated by Eq. (15) and Eq. (17) will rise; for this reason, we add Eq. (16) and Eq. (18) to avoid virtual stiffness overflow.

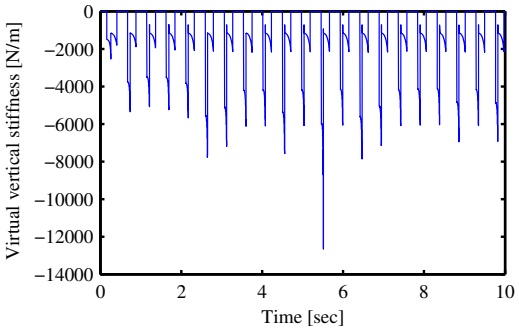

Figure 13. The evolution of the vertical stiffness of the virtual model during hopping with horizontal velocity at 2 m/s

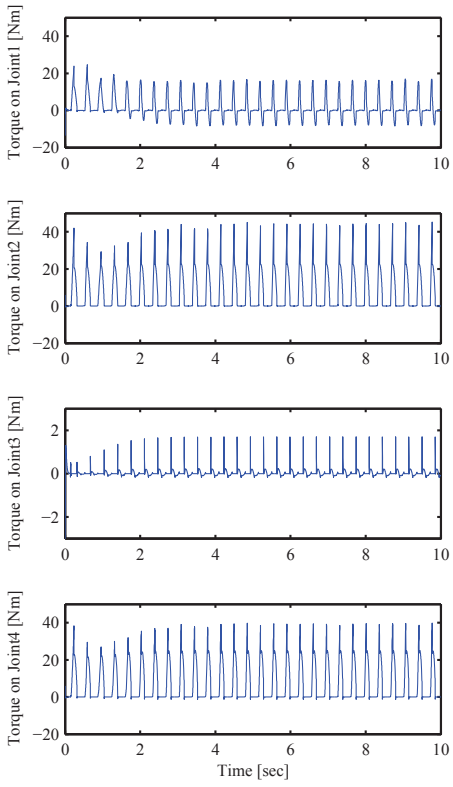

Figure 14. The torques on the four joints; joint 3 is passive during the supporting phase and active during the swing phase

The torques of the four joints are shown in Figure 14. During the swing phase, the joint torque outputs are all very low to keep the feet positions steady. The feet are compliant enough to touch but not crush onto the ground. Discontinuity of the curves is caused by changes in the stiffness between the compressing period and releasing period in the supporting phase.

5.3 Robustness study with different leg masses

The previous simulations are based on the assumption of the control approach presented in section 3.1 and with a very low mass ratio of leg/torso (1:500). But what will happen if this assumption is not satisfied? To test the performance of the control approach in this paper with different leg link masses, we conducted two experiments using different mass ratios (1:50 and 1:5).

When each leg link mass is 0.05kg and the torso mass is 5kg, the parameters are the same as in the simulation with a leg link mass of 0.005kg, for except h_d. Since the robot becomes heavier, the h_d is increased for a more desired input energy. The CoM velocity and position curves of the robot torso on three axes are shown in Figure 15. Although the horizontal velocity error is larger than the error in the experiment with the leg link mass at 0.005kg and the vibration of the torso pitch becomes more severe, the robot can still hop at a speed of 2m/s.

Parameter	*Unit*	*Value*
h_d	m	1.2
h_0	m	0.65
h_s	m	0.75
h_{sz}	N·m/rad	1100
k_{dx}	N·m/(rad·s^{-1})	29
μ_{xy}	1	0.1
μ_{zy} (during Compressing Period)	1	0.19
μ_{zy} (during Releasing Period)	1	0.19
k_v	N/(m·s^{-1})	80
k_{SV}	m/(m·s^{-1})	0.11

Table 4. The parameters used in hopping control with a leg link mass of 0.5kg and a desired horizontal velocity (v_d) of 2m/s

When the leg link mass is raised to 0.5kg, the mass ratio of leg/torso is raised to 1:5 and the rotation of the torso pitch angle cased by the swing leg cannot be ignored any longer in the swing phase. We have to set the desired torso's pitch angle at 0.15 rad to compensate for the rotation of the torso in the swing phase and the control parameters for doing so are shown in Table 4. The vibration of the torso's pitch angle is very strong, but there is no change in the control approach. The results of the experiment with a leg mass of

0.5kg are shown in Figure 16. The vibration of the torso pitch becomes much more severe than in previous experiments. Another simulation of 40 seconds shows that the hop merges into a cyclic motion and the robot runs steadily.

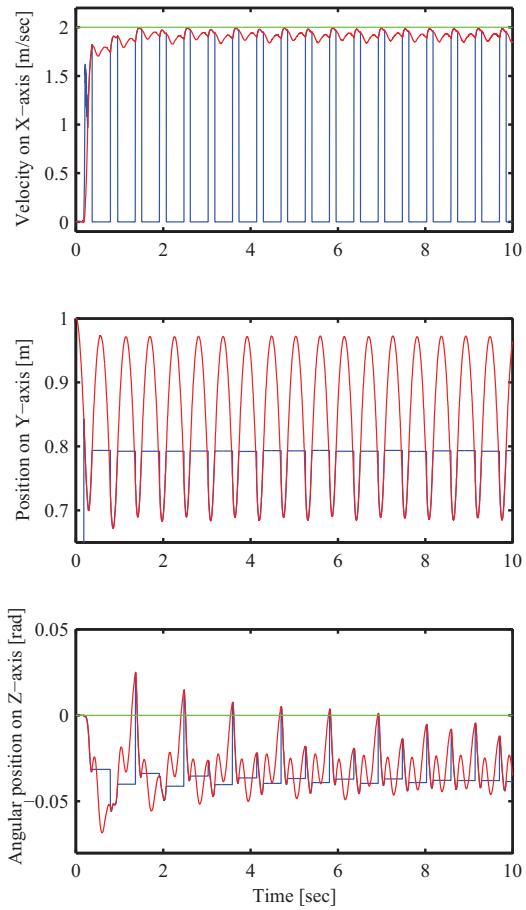

Figure 15. With a leg link mass of 0.05kg, the velocity and position curves of the robot torso's CoM is shown during the hop. The desired horizontal velocity (v_d) is 2 m/s. The curves drawn in red are the values measured by the two guides, the blue curves are calculated by the forward kinematics and the green curves are the desired values.

A demo of the experimental results can be viewed at the following URL: http://v.youku.com/v_show/id_XMTM1NTA2MTAyMA==.html.

6. Conclusions and Discussions

In this paper, we presented a planar hopping control approach using a virtual model and energy planning based on trotting gait. Using this approach, the planar motions of the robot's torso are decoupled and fully controllable in the supporting phase. The proposed hopping control approach is verified by simulated experiments. A number of conclusions are drawn as follows.

Firstly, this approach is easy to implement using a micro controller since computation complexity is very low. In the hopping control, stiffness on the y -axis is generated by the energy of the virtual model; this calculation highly depends

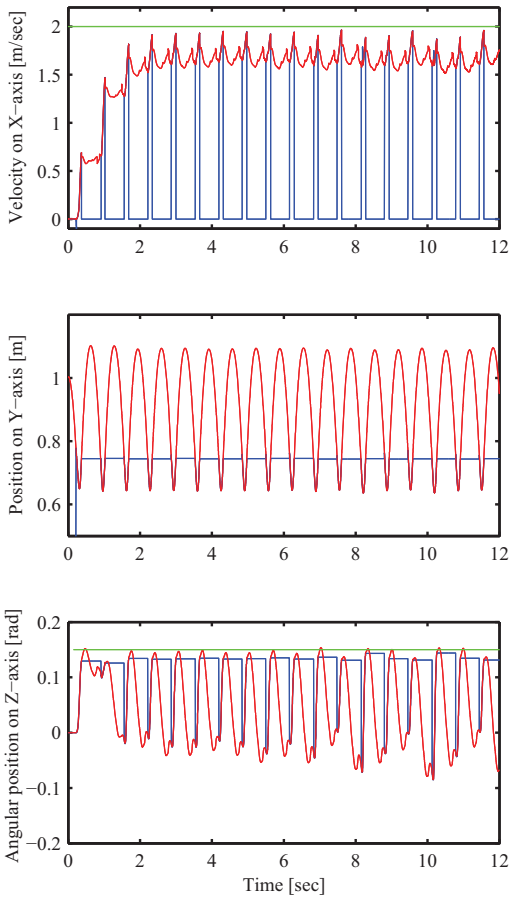

Figure 16. With a leg link mass of 0.5kg, the velocity and position curves of the robot torso's CoM is shown during hopping. The desired horizontal velocity (v_d) is 2 m/s. The curves drawn in red are the values measured by the two guides, the blue curves are calculated by the forward kinematics and the green curves are the desired values.

on kinematics and velocities and as such the calculation is simpler than using a dynamics model, and the controller does not require high computing capabilities for real-time control.

Secondly, gait is generated by the planned energy and contact status of the feet, and is more adaptable to the environment than gait planning based on time. A single leg remains in the swing phase when the foot touches the ground, except in the case of low stiffness or driving force. Motion control of the foot with low stiffness in the swing phase can effectively reduce impact when unexpected contact occurs between the foot and ground. When the gait is switched from the swing phase to the supporting phase, both feet of the robot touch on the ground, and the virtual vertical stiffness takes effect. When the gait is switched from the supporting phase to the swing phase, one foot takes off from the ground, the virtual vertical stiffness gets unavailable. Therefore, gait can be aperiodic.

Thirdly, the mass of the legs will affect the performance of the hopping control, particularly in the swing phase. This is also a factor for other control models such as the SLIP

model. In addition, control based on the dynamics model is too complex for calculating real-time control. Many researchers have made significant efforts to reduce the leg/torso mass ratio to solve this problem [5, 14]. In this paper, as the simulation demonstrates, the hopping control method is available when the leg/torso mass ratio is 1:5; however the parameters must be adjusted and the vibration of the torso pitch angle is extremely severe in this instance.

Finally, we used a group of high impedance parameters to maintain the angular position of the torso's posture. Thus, the vibration of the torso's pitch angle was weak during hopping.

However, the high impedance parameters resulted in lower posture stability and higher joint torques. k_{sz} and k_{dz} were set based on the amplitude of the vibration of the pitch angle of the torso and the output torques on joints. The higher the k_{sz} and k_{dz}, the weaker the amplitude of pitch vibration was. This also increased the output joint torque. Thus, we set k_{sz} and k_{dz} as small as possible to maintain the amplitude of the pitch vibration at less than 0.03 rad (approximately 2 degrees). This rendered the hopping process extremely sensitive to changes in parameters with a higher horizontal speed. In future research, we aim to improve the control model for the torso's posture, lower the impedance parameters using a rhythmic vibration to achieve a higher running speed and optimize these two parameters automatically.

7. Acknowledgements

This work is partially supported by the National Natural Science Foundation of China (6123301), National High Technology Research and Development Program of China (2015AA042201).

The authors gratefully acknowledge the help and discussion provided by Professor Wei Zhang and Yan Li from the School of Control Science and Engineering, Shandong University. We appreciate all their efforts in the writing of this paper.

8. References

[1] Kajita S, Espiau B (2008) Legged robots. In: Siciliano B, Khatib O. Springer Handbook of Robotics. Berlin: Springer. pp. 361-389.

[2] Li Y, Li B, Ruan J, Rong X (2011) Research of mammal bionic quadruped robots: A review. In: 2011 IEEE International Conference on Robotics, Automation and Mechatronics (RAM). 2011 Sep 17-19; Qingdao, China. IEEE. pp. 166-171.

[3] Raibert M, Blankespoor K, Nelson G, Playter R (2008) BigDog, the rough-terrain quadruped robot. In: Proceedings of the 17th IFAC World Congress. 2008 Jul 6-11; Seoul, South Korea. IFAC. pp. 10822-10825.

[4] Wikipedia Legged squad support systems [Internet]. Sept 2012 [updated 11 Feb 2015; cited 29 Apr 2015]. Available from: http://en.wikipedia.org/wiki/Legged Squad Support System. Accessed on 29 Apr 2015.

[5] Semini C (2010). HyQ - Design and development of a hydraulically actuated quadruped robot [PhD thesis]. Italy: University of Genoa.

[6] Ugurlu B, Havoutis I, Semini C, Caldwell DG (2013) Dynamic trot-walking with the hydraulic quadruped robot - HyQ: analytical trajectory generation and active compliance control. In: 2013 IEEE/RSJ International Conference on Intelligent Robots and Systems (IROS). 2013 Nov 3-7; Tokyo, Japan. IEEE. pp. 6044-6051.

[7] Cho J, Kim JT, Park S, Kim K (2013) Dynamic walking of JINPOONG on the uneven terrain. In: 2013 10th International Conference on Ubiquitous Robots and Ambient Intelligence (URAI). 2013 Oct 30 - Nov 2; Jeju, South Korea. IEEE. pp. 468-469.

[8] Chai H, Meng J, Rong X, Li Y (2014) Design and Implementation of SCalf, an Advanced Hydraulic Quadruped Robot. ROBOT. 36(4): 385-391.

[9] McGhee R B (1968) Some finite state aspects of legged locomotion. Mathematical Biosciences. 2(1): 67-84.

[10] Raibert MH (1986) Legged robots that balance. Cambridge, MA: MIT Press, p. 233.

[11] Ahmadi M, Buehler M (1997) Stable control of a simulated one-legged running robot with hip and leg compliance. IEEE Transactions on Robotics and Automation. 13(1): 96-104.

[12] Sato A, Buehler M (2004) A planar hopping robot with one actuator: design, simulation, and experimental results. In: Proceedings of the 2004 IEEE/RSJ International Conference on Intelligent Robots and Systems, (IROS). 2004 Sept 28 - Oct 2; Sendai, Japan. IEEE. Vol. 4, pp. 3540-3545.

[13] Smith JA, Poulakakis I (2004, September). Rotary gallop in the untethered quadrupedal robot scout II. In: Proceedings of the 2004 IEEE/RSJ International Conference on Intelligent Robots and Systems, 2004. (IROS 2004). 2004 Sept 28 - Oct 2; Sendai, Japan. IEEE. Vol. 3, pp. 2556-2561.

[14] Ananthanarayanan A, Azadi M, Kim S (2012) Towards a bio-inspired leg design for high-speed running. Bioinspiration and biomimetics. 7(4): 913-929.

[15] Seok S, Wang A, Chuah MY, Otten D (2013) Design principles for highly efficient quadrupeds and implementation on the mit cheetah robot. In: 2013 IEEE International Conference on Robotics and Automation (ICRA). 2013 May 6-10; Karlsruhe, German. IEEE. pp. 3307-3312.

[16] Valenzuela AK, Kim S (2012) Optimally Scaled Hip-Force Planning: A control approach for quadrupe-

dal running. In: 2012 IEEE International Conference on Robotics and Automation (ICRA). 2012 May14-18; Saint Paul, MN. IEEE. pp. 1901 - 1907.

[17] Shkolnik A, Levashov M, Manchester IR, Tedrake R (2010) Bounding on rough terrain with the LittleDog robot. International Journal of Robotics Research, 30(2): 192-215.

[18] Boston Dynamics (2013) CHEETAH - Fastest Legged Robot [Internet]. [updated 2013; cited 29 Apr 2015]. Available from: http://www.bostondynamics.com/robot_cheetah.html. Accessed on 29 Apr 2015.

[19] Pratt J, Torres A, Dilworth P, Pratt G (1996) Virtual Actuator Control. In: Proceedings of the 1996 IEEE/RSJ International Conference on Intelligent Robots and Systems (IROS). 1996 Nov 4-8; Osaka, Japan. IEEE. Vol. 3, pp.1219-1226.

[20] Pratt J, Chew C M, Torres A, Dilworth P, Pratt G (2001) Virtual model control: an intuitive approach for bipedal locomotion. International Journal of Robotics Research, 20(2): 129-143.

[21] Pratt G, Williamson M (1995) Series elastic actuators. In: Proceedings of the 1995 IEEE/RSJ International Conference on Intelligent Robots and Systems (IROS). 1996 Aug 5-9; Pittsburgh, PA. IEEE. Vol. 1, pp. 399-406.